J. Agr. Sci. Tech. (2022) Vol. 24(3): 603-616

Investigation of Operating Performance of Single-Side Paddy Field Ridger Based on Discrete Element Method and Test Verification

M. Liu[1]*, C. Hu[1], H. Ku[1], and H. Cai[1]

ABSTRACT

In order to improve the quality and efficiency of a ridger and explore the effect of working condition on its performance, a coupling model of the key components of a single-side paddy ridger and soil was proposed based on discrete element method. Then, with the working parameters of the ridger as experimental factors and its soil firmness and torque as the evaluation indicators, an orthogonal test was designed, and a parameter optimization was conducted through response surface analysis method. The optimal working conditions were set as follows: forward speed of the machine at 0.3 m s^{-1}, rotational speed of rotary tillage at 500 rpm, and the working depth of the rotary tillage at 200 mm. The corresponding soil firmness was 2,592.58 kPa, and the working torque of the rotary cutting soil and compacting ridger device was 255.1 and 360.1 N m, respectively. Finally, a torque calibration test on the compacting ridger device was conducted and a mathematical model of the torque measurement was established. By comparing the simulation optimization and experimental results, the relative error of the output torque of the compacting ridger device was 4.77%, and that of the ridge soil firmness was 6.77%.

Keywords: Rice mechanization**,** Side ridger, Soil firmness, Torque calibration.

INTRODUCTION

Paddy field construction is an important part of the mechanization of rice production. Soil performance parameters have a significant impact on operational power consumption (AshrafiZadeh, 2006). Godwin *et al*. (2007) predicted the draught of the plow body by a mathematical model, which showed the relationship between the depth and number of plough bodies as well as the power of the tractor, meanwhile the reliability of the model was determined through experiments. Bery *et al*. (2019) studied the characteristics and behavior of clayey sand soil through a series of experiments such as shear tests, which provided a basis for subsequent research on soil. Asaf *et al*. (2006) preformed a simulation of biaxial tests and the calculation of the internal angle of friction and cohesion through a two-dimensional discrete-element model. It was found that discrete element was a very effective method for complex soil interaction. Karmakar *et al*. (2009) simplified the soil into a Bingham material and simulated the soil mechanical behavior through Computational Fluid Dynamics (CFD) approach. In the past decades, Discrete Element Method (DEM) has been widely adopted for the construction of a high-fidelity model to describe the soil–tillage interaction (Bravo *et al*., 2014; Shmulevich, 2010). By coupling with a Linear Cohesive force Model (LCM) into a delayed elastic Contact Model (HSCM), Ucgul *et al*. (2014,

[1] Hubei Agricultural Machinery Engineering Research and Design Institute, Hubei University of Technology, Wuhan430068, People Republic of China.
*Corresponding author; e-mail: lmy8508@hbut.edu.cn

and 2015) established a soil particle contact model and solved the problem of soil stress plastic deformation. Sukhbir Singh *et al*. (2017) studied the effect of different types of furrow opener at different depth and speed of operation on soil penetration resistance, ridge height, specific draft, and soil disturbance and germination percentage to select the best furrow opener for establishment of sugarcane crop. Zheng *et al*. (2017) designed a combined counter-rotating tillage tool, and optimized the execution parameters through discrete element method and finite element analysis, through which the best working condition was obtained. Mao *et al*. (2012) analyzed the main influencing parameters of the power consumption of a rotary tiller, and established a mathematical model of its dynamics to provide an effective theoretical plan for future research on rotary tillers. Wang *et al*. (2017 and 2019) designed the 1DSZ-350 suspended paddy field single-sided construction machine, systematically analyzed the dynamic changes in the power of the machine and its power consumption through discrete element method, providing an effective theoretical support for optimized design of bridging machines in the future. Wang *et al*. (2017, 2019) designed a two-way car repair machine for rice fields, which could realize 180-degree reversal and made the functions of the existing bridge construction machines more diversified, providing a direction for the future design of new types of bridge construction machines.

Many scholars have studied the performance of the ridge machine by experiment. In view of the complexity of soil model, few studies using theoretical methods have been reported. In this study, we aimed to use the discrete element method to establish a coupling interaction model between the key components of a single-side ridger and the soil and obtain the variation of soil-tool interaction force and operating torque. Also, we planned to determine the optimal operating parameters by using an orthogonal test and the response surface analysis method, to achieve the maximum soil firmness and the minimum operating torque and verify the correctness of the numerical simulation through a field test.

MATERIALS AND METHODS

The core operating parts of the 1ZG-350 single-side paddy field ridger consisted of a compacting ridger device (No. 8 in Figure 1) and a rotary tiller device (No. 9). By adjusting the height of the handle (No. 7) and horizontal hydraulic cylinder (No. 12), the agronomic requirements on the ridger could be met. The traction power was transferred to rotary tiller device (No. 9) through power transmission shaft (No. 2) and chain transmission part (No.5) and to compacting ridger device through commutation gear box (No. 4) and universal joint (No. 10). Rotary tiller device performed the operation of rotary soil tillage and the soil collecting. Compaction ridger device performed operation of compacting ridger.

Geometric Analysis of Field Ridge

According to agronomic requirements, the height of ridger $H \geq$ 250 mm, and the corresponding ridger firmness should be greater than 1,500 kPa. As in Figure 2, the complete cross-sectional area S_1 of the ridger was given as:

$$S_1 = (q + w) \cdot H / 2 \quad (1)$$

Where, q, w and H are the width of ridger base, width of ridger roof and the height of the ridger respectively.

The cross-sectional area of rotary cutting soil S_2 is expressed as:

$$S_2 = R^2\theta - BR \cdot \cos\theta / 2 \quad (2)$$

Where, R is rotary radius of the rotary cutter, B is the width of soil, and $\theta = \arcsin(B/2R)$ is the contact angle between the cutter and soil.

Considering the role of soil compaction, the relationship between the rotary cutting

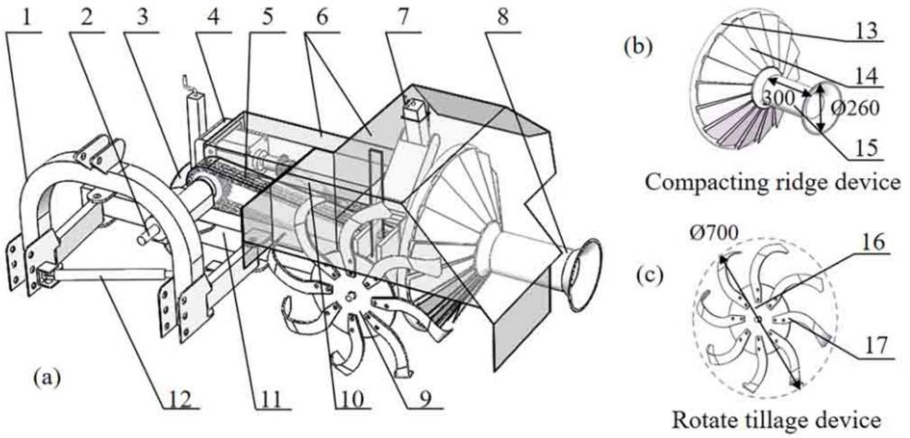

Figure 1. Schematic diagram of 1ZG-350 single-side ridger: 1. Traction frame; 2. Power transmission shaft; 3. Directional wheel; 4. Commutation gear box; 5. Chain transmission part 6; Hood; 7. Height adjustment handle; 8. Compaction ridge device; 9. Rotary tillage device; 10. Universal joint; 11. Rack; 12. Hydraulic cylinder; 13. Vane mounting rack; 14. Elastic vane; 15. Compaction roller; 16. Cutter disc; 17. Rotary cutter (dimension in mm).

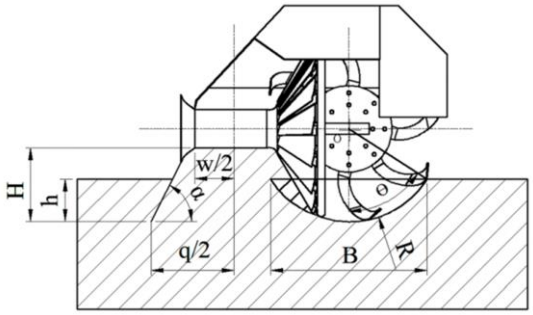

Figure 2. Schematic diagram of rotary cutting soil and compacting ridger.

soil and cross-sectional area of the ridger can be expressed as:

$$S_1 = k[2S_2 + h(q - h \cdot \cot \alpha)] \quad (3)$$

Where, k is the coefficient of soil firmness, h is the rotary tillage depth, and α is the slope angle of ridger-type.

In this study, geometric parameters of the ridger designed were H= 300 mm, w= 350 mm, q= 720 mm and α= 60°. The corresponding rotary tillage depth h, rotary radius of rotary cutter R and soil firmness coefficient k were set as 200 mm, 400 mm, and 0.95, respectively. Then, the theoretical width of soil B was equal to 467 mm.

To accurately describe the interaction of soil and machine, an integrated Linear Cohesion Model (LCM) and a delayed elastic Contact Model (HSCM) was established (Ucgul *et al*., 2014 and 2015). For the interaction among soil particles, normal and tangential interaction could be simplified as a spring and damping system. The total normal force could be expressed as:

$$F_N = F_n + F_c = k_n\delta + c_n\dot{\delta} + F_c \quad (4)$$

Where, k_n, c_n are normal stiffness and damping, respectively, δ is the normal approach. $F_c = A_c \cdot \xi$, ξ is the cohesion, A_c is the action area of soil and ξ is the cohesion coefficient.

Tangential forces among soil particles can be given as:

$$F_t = \min(k_t\delta + c_t\dot{\delta}, \mu_n F_N) \quad (5)$$

Where, k_t, c_t are tangential stiffness and damping respectively and μ_n is the coefficient of soil internal friction.

Similarly, the corresponding total normal and tangential force between soil and the machine can be expressed as:

$$F'_n = F'_n + F' = k'_n\delta + c'_n\dot{\delta} + F' \quad (6)$$

$$F'_t = \mu_w F'_n + \mu' F' A' \quad (7)$$

Where, k'_n, c'_n are normal stiffness and damping respectively, F' is the additional normal force generated by the adhesion, μ_w is the friction coefficient between soil and the machine, μ' is the adhesion coefficient, and A' is the adhesion area.

Besides, soil performance parameters whose corresponding test site is shown in Figure 3 should be measured. As shown in Figure 4, the results of soil sieving showed that the soil particle size of 0.25 ~ 8 mm accounted for 88.9% of the total number of soil samples. The measured friction angle of soil was 15°, and the cohesion among soil particles was 22.23 kPa, as shown in Figure 5. Relevant parameters of the soil and machine are presented in Table 1.

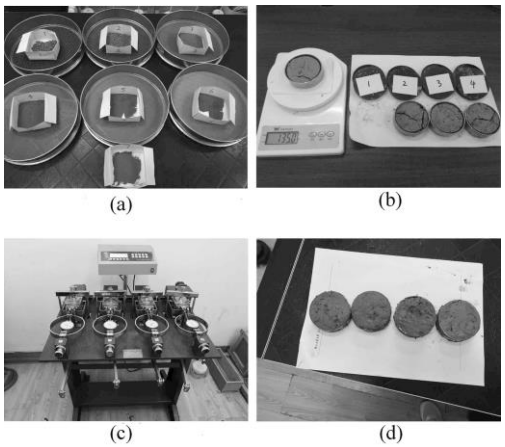

Figure 3. Test experiment of soil parameters: (a) Screening method to measure the distribution of soil particle size: (b) Ring knife method to measure soil bulk density; (c) ZJ strain control direct shear, (d) Direct shear test.

Simulation Analysis of Single-Side Ridger

The simulated soil-box was 2,000 mm in length, 1,300 mm in width, and 400 mm in height, and the production rate of soil particles was 1.0×10^5 per second, the total simulation time was 13 seconds and time step was set as 3.5×10^{-5} seconds. In this section, the corresponding operating conditions were set as follows: the forward speed of the machine was 0.3 m s^{-1}, the rotational speed of rotary tillage was 540 rpm and the depth of rotary tillage was 200 mm. The simulation process is shown in Figure 6.

Figure 7 shows that the ridger interacted with the soil after 7 seconds. The corresponding interaction force and working torque increased gradually and tended to be

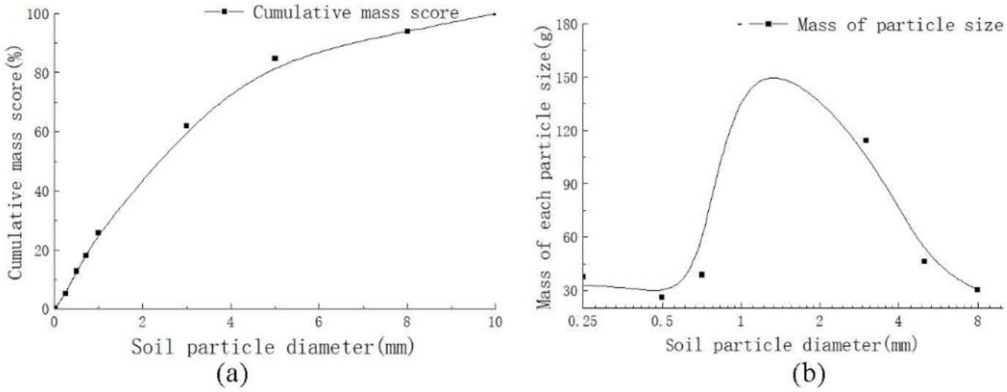

Figure 4. Measurement results of the distribution of soil particle size: (a) Curve of cumulative percent content on sieve, (b) Distribution curve of soil particle size.

the

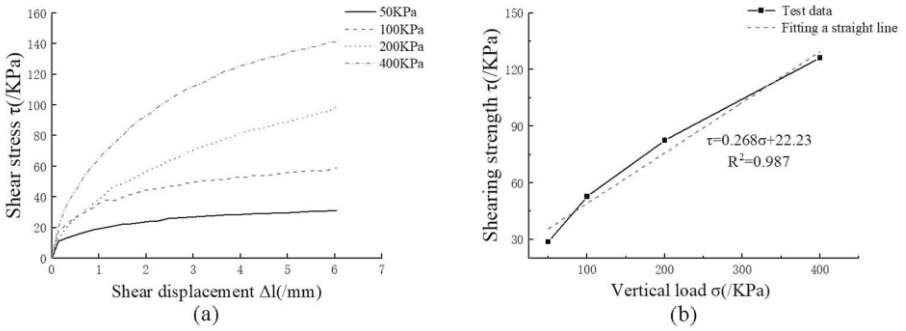

Figure 5. Results of soil direct shear test: (a) Curve of shear stress and shear displacement, (b) Relationship between shear strength and vertical load.

stable after 8.5 seconds. It was also shown that after 8 seconds, both soil-machine interaction force and the torque applied to the compacting ridger device were greater than those applied to the rotary tillage device in Figure 7. The rotary cutters mainly overcame the internal friction and cohesion of soil particles. Due to action of compaction and larger contact area among soil particles, the compacting roller and the elastic vane, the soil-machine interaction force and the working torque were kept at 2272.96 N and 372.24 N□m, respectively. The variation trend of soil-machine interaction force and the working torque of rotary tillage device were similar to that of compacting ridger device. The corresponding value of soil-machine interaction force and the working torque was kept at 657.57 N and 258.91 N m, respectively.

Table 1.Material properties and contact parameters.

Parameters	Value
Poisson's ratio of soil	0.33
Density of soil (kg m^{-3})	2680
Particle size distribution (mm)	0.25-8
Elastic module of soil (MPa)	35
Shear modulus of soil (MPa)	25
Coefficient of restitution of soil-soil (ξ)	0.6
Coefficient of static friction of soil-soil (μ_s)	0.6
Coefficient of rolling friction of soil-soil (μ_r) (μ_w) (μ_w)	0.4
Poisson's ratio of 65 Mn	0.35
Poisson's ratio of 45 Steel	0.31
Density of 65 Mn (kg m^{-3})	7850
Density of 45 Steel (kg m^{-3})	7800
Elastic module of 65 Mn (MPa)	1.97×0^5
Elastic module of 45 Steel (MPa)	2.1×10^5
Shear modulus of 65 Mn (MPa)	7.8×10^5
Shear modulus of 45 Steel (MPa)	7.0×10^5
Coefficient of restitution of soil-45 Steel	0.6
Coefficient of restitution of soil-65Mn	0.6
Coefficient of static friction of soil-45 Steel	0.5
Coefficient of static friction of soil-65 Mn	0.5
Coefficient of rolling friction of soil-45 Steel (μ_w) (μ_w)	0.05
Coefficient of rolling friction of soil-65 Mn (μ_w) (μ_w)	0.05
Adhesion coefficient of soil-65 Mn	0.45
Adhesion coefficient of soil-45 Steel	0.45

RESULTS AND DISCUSSION

EDEM Virtual Simulation Experiment and Parameter Optimization Analysis

Design of Virtual Simulation Experiment

In order to reveal the influence of operating condition on the performance of the ridger, an orthogonal experiment was carried out based on the discrete element model proposed. In the current study, the forward speed (A), rotational speed of rotary tillage (B), and the depth of rotary tillage (C) were selected as experimental factors. The firmness of the ridger and the working torque of its key components were adopted as the evaluation indicators. The scheme of virtual simulation experiment was designed through a three-factor and four-level orthogonal experiment (Chen *et al.*, 2019).

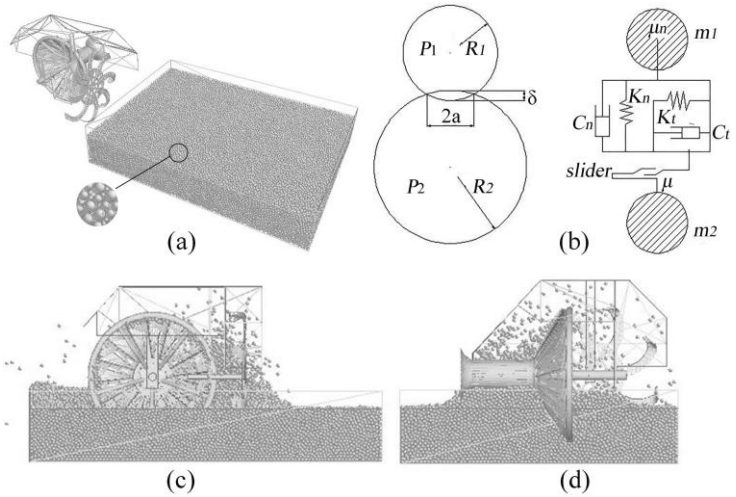

Figure 6. Simulation process of the single-side ridger: (a) Soil particle sedimentation; (b) Soil particle model; (c) Rotary cutting of soil, (d) Compression and construction of the ridger.

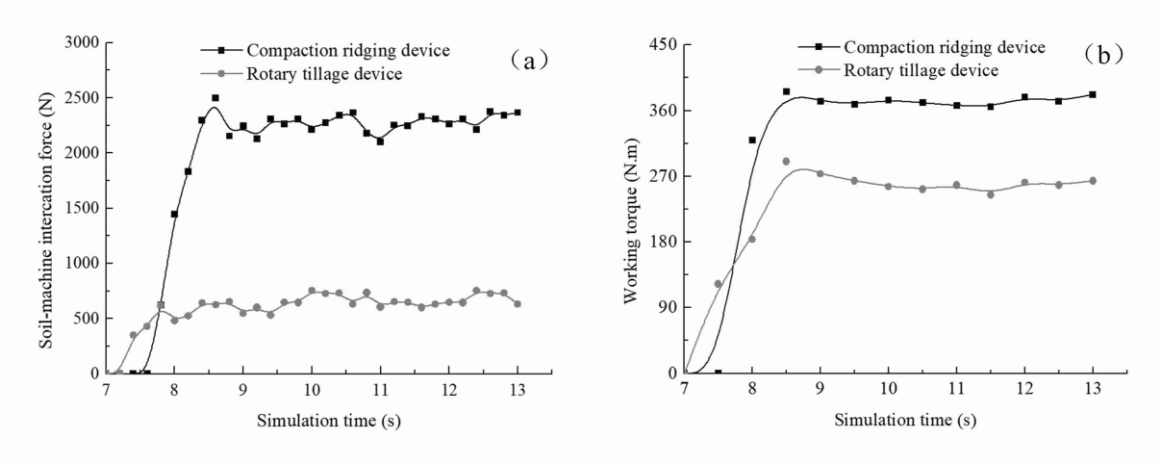

Figure 7. Variation of soil-machine interaction force and working torque.

The L16 (45) orthogonal table was adopted, and the corresponding parameters as well as levels of working parameters are shown in Table 2.

Parameter Optimization Analysis Based on Virtual Simulation Experiment

The firmness parameter cannot be extracted directly from EDEM software, but it can be obtained through the soil compaction calibration method. The quantitative amount of soil with an initial water content of 23.28% was added to a container and mixed evenly. The soil firmness under different loads was measured by loading various weights, as shown in Figure 8. The corresponding measurement data and fitting curve are shown in Figure 8 (c). The expression of fitting curve between the soil firmness *S* and the loading force *F* is given as follows：

$$S = 1.293F - 63.2 \quad (8)$$

As shown in Table 3, the optimal combination of parameters of the soil firmness and operating torque was inconsistent. To obtain the best combination of operating parameters, multi-objective variable optimization method was applied to the results of the orthogonal experiment. Expression of the mathematical model can be given as follows:

$$\begin{cases} \max S \\ \min T \\ s.t.\ \ 0.2\,m/s \le \mathrm{x}_1 \le 0.5 m/s \\ \quad 400\,r/min \le x_2 \le 700 r/min \\ \quad 140\,mm \le x_3 \le 200 mm \\ \quad 1500\,\mathrm{kPa} \le S(x_1, x_2, x_3) \le 3000\,\mathrm{kPa} \\ \quad 0 \le T(x_1, x_2, x_3) \le 700 N \cdot m \end{cases} \tag{9}$$

Where, Variables x_1, x_2 and x_3 are the forward speed, the rotational speed of rotary tillage, and the depth of rotary tillage, respectively.

The optimization model described in Equation (9) can be solved through the Response Surface Method (RSM) (Diletta *et al*., 2020). Then, the optimal combination of parameters could be obtained as A2B2C4. The corresponding forward speed, the rotational speed of rotary tillage, and the depth of rotary tillage were 0.3 m s^{-1}, 500 rpm, and 200 mm, respectively. Meanwhile, firmness of the ridger was 2635.84 kPa, and the working torque of rotate tillage device and compaction device was 267.89 and 365.54 N m, respectively. To verify the reliability of the optimization results, the parameter optimization results were calculated and verified through discrete element method. Firmness of the ridger and working torque of the key components of the machine were obtained as 2592.58 kPa, 255.02 N m, and 360.11 N m, respectively. The relative errors of ridge firmness and working torque were 1.64 and 2.89%, respectively.

Experimental Investigation and Verification

Torque Calibration Test of the Compaction Device

Firmness of the paddy field ridger was measured by the SL-TSC multi-parameter firmness tester, whose torque was measured

through a strain test. Due to the complex structure of the compacting ridger device, a

Table 2. Experimental factor levels of operating condition.

Level	Forward speed (A) (m s^{-1})	Rotary speed (B) (rpm)	Depth of rotary tillage (C) (mm)
1	0.2	400	140
2	0.3	500	160
3	0.4	600	180
4	0.5	700	200

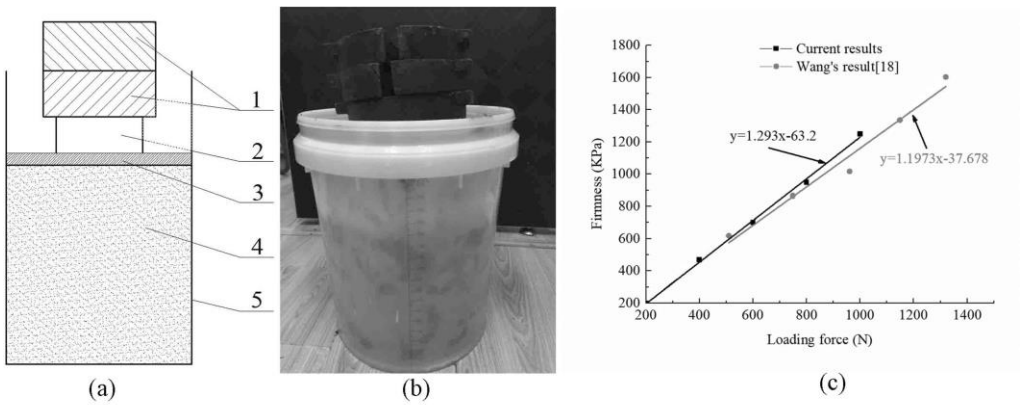

Figure 8. Soil compaction calibration test: 1. Weight; 2. Partition; 3. Bearing plate; 4. Soil; 5. Measuring cylinder; (a) Calibration principle; (b) Field test, (c) Data fitting curve.

Table 3.Orthogonal experimental scheme and results.

	Test factor			Test index			
					Torque (N m)		
NO.	A	B	C	Firmness (kPa)	Rotary cutter	Cracking wheel	Total torque
1	1	1	1	1915.2	241.4	339.4	580.8
2	1	2	2	2230.9	253.5	343.6	597.1
3	1	3	3	2388.7	255.1	361.8	616.8
4	1	4	4	2687.6	251.9	355.2	607.1
5	2	1	2	2317.9	245.5	368.4	613.9
6	2	2	1	2364.9	248.9	355.1	604.1
7	2	3	4	2747.4	256.3	379.9	636.2
8	2	4	3	2451.6	269.2	389.8	659.1
9	3	1	3	2691.3	255.7	391.5	647.2
10	3	2	4	2506.6	266.1	367.7	633.8
11	3	3	1	2194.9	260.2	377.6	637.8
12	3	4	2	1964.8	238.3	362.6	600.9
13	4	1	4	2372.2	234.9	368.7	603.6
14	4	2	3	2561.1	229.1	381.7	610.8
15	4	3	2	2368.9	240.1	387.2	627.2
16	4	4	1	2296.6	271.9	399.4	671.4
	K1	9219.3	9295.7	8769.7			
	K2	9879.1	9661.6	8852.5			
SS	K3	9328.8	9697.9	10090.7			
	K4	9598.7	9370.7	10312.9			
	R	659.7	402.2	1543.3			
	Primary and secondary order		C> A> B				
	Optimal level		A2、B3、C4				
	Optimal combination		A2B3C4				
	K1	2401.8	2445.5	2494.0			
	K2	2513.2	2445.7	2439.0			
TT	K3	2519.5	2517.9	2533.8			
	K4	2513.0	2538.4	2480.7			
	R	117.8	92.9	94.8			
	Primary and secondary order		A> C> B				
	Optimal level		A1、B1、C2				
	Optimal combination		A1B1C2				

calibration test was carried out before measuring the field torque. Five measuring points were evenly distributed in the circumferential direction of a certain radius of the rotary disc in the compacting ridger device. For each measuring point, a 1/4 bridge test circuit was built by the multi-channel digital strain meterTMR-211, as shown in Figure 9.

As shown in Figure 9, the torque at six levels could be obtained through step-by-step loading method. The weight of each increase was 10.2 kg, and the corresponding increment of torque was 33.99 N m. Figure 10 shows the change of strain with time at the five measuring points while the loading torque was 197.92 N m.

As shown in Figure 10, the strain value of each measuring point gradually increased during the loading process of 4.5-5 seconds, which tended to be stable after 5 seconds. Under various loading levels, the mean value of the steady-state strain of each measuring point was plotted according to the

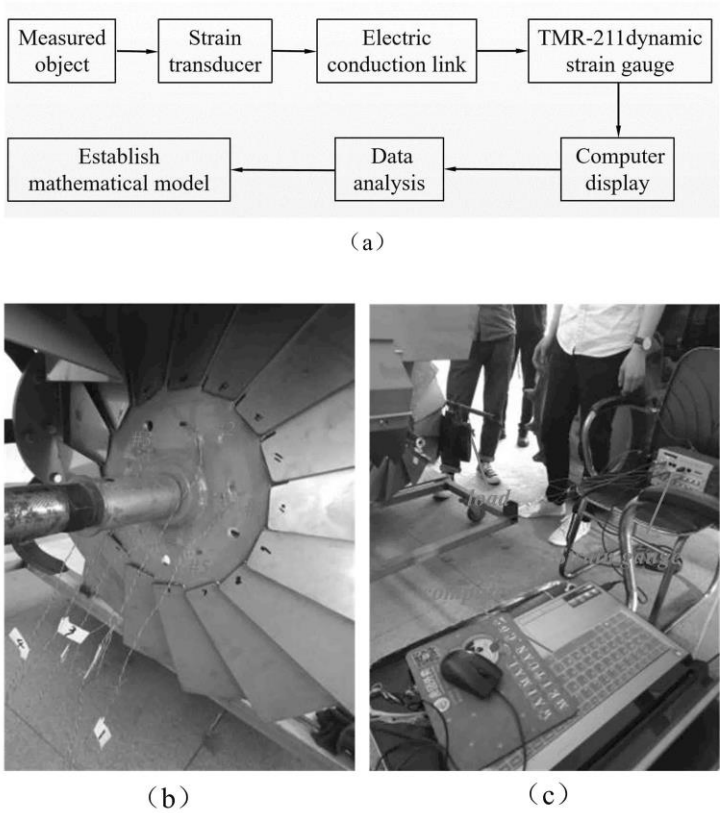

Figure 9. Torque calibration experiment of the compacting device: (a) Block diagram of torque calibration test system; (b) Strain gauge paste physical map, (c) Test site.

position phase of the above measuring points (Figure 10-b). It is indicated that the variation of strain with the phase of measuring positions was a kind of sinusoidal wave. As the load increased, the amplitude of the curve also increased.

To calibrate the relationship between the torque and the strain of the compacting ridger device, the amplitude of strain sinusoidal curve at each measuring point was extracted. Then, the relationship between the strain amplitude and the loading torque was obtained through data fitting, as shown in Figure 11. The correlation coefficient of curve fitting R was 0.985, and the corresponding relationship can be expressed as Equation (10):

$$T = 9.809x + 9.429 \quad (10)$$

Where, T is the torque of compacting device and x represents the strain amplitude at measuring points.

Field Test of Single-Side Paddy Field Ridger

To verify the reliability of the results of virtual simulation and optimization, an experimental study was carried out under the optimal combination of working parameters (Figure 12). Since measuring point 1-5 went through a similar process during operation, measuring points 1, 3, and 5 were selected for the torque test on the compacting ridger device. The initial soil firmness measured was between 250 and 450 kPa, soil density was 2,860 kg m^{-3}, and water content was 20-25%. The above parameters met the operational requirements of agronomy.

The operation parameters were set as follows: the forward speed was 0.3 m s^{-1}, the

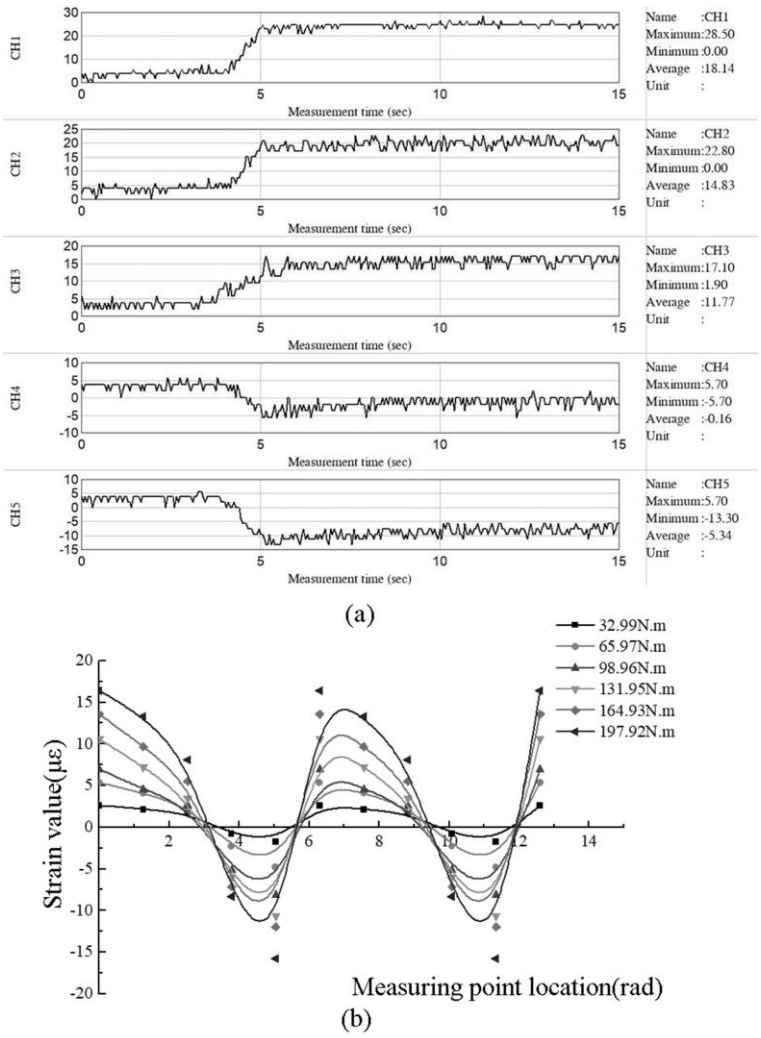

Figure 10. Torque calibration test results: (a) Variation of strain with time at the five measuring points under the torque of 197.92 N m, (b) The strain curve with the position of the measuring points with different torques.

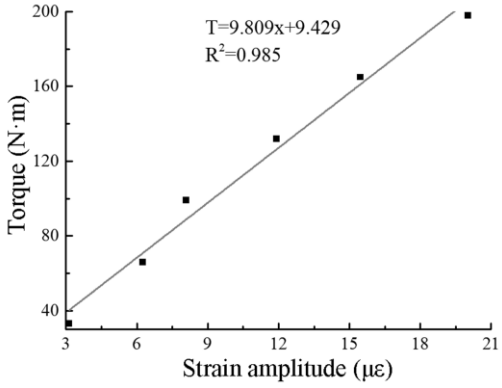

Figure 11. Fitting curve of load torque versus strain amplitude.

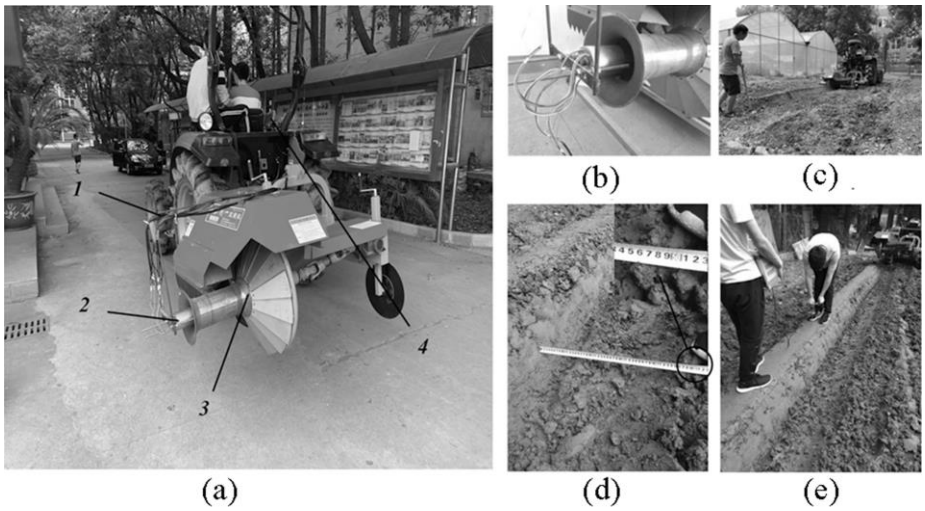

Figure 12. Field test of single-side ridger: 1. Cage; 2. Electric conduction link; 3. The device under test; 4. Computer display; (a) Mark drawing of the test equipment; (b) Repression of device torque building test; (c) Machine test process; (d) Rotary tillage width measurement, (e) Firmness measurement.

rotational speed of rotary tillage was 500 rpm, and the depth of rotary tillage was 200 mm. The whole process is shown in Figure 12 (c). Figures 14-d and -e show the measurement of soil width for rotary tillage and that of soil firmness of the ridger, respectively. Figure 13 shows the variation of strain with time at the measuring points 1, 3, and 5. Such a phenomenon was consistent with the result of calibration test. Based on a field test and a torque calibration test, relevant geometric and mechanical parameters of the ridger are given in Table 4. It can be seen that all technical indexes of the ridger met agronomic requirements. For example, relative error of the output torque of the compacting device was 4.77% and that of the firmness of the ridger was 6.77%. According to the results, the same conclusion was obtained in the experimental

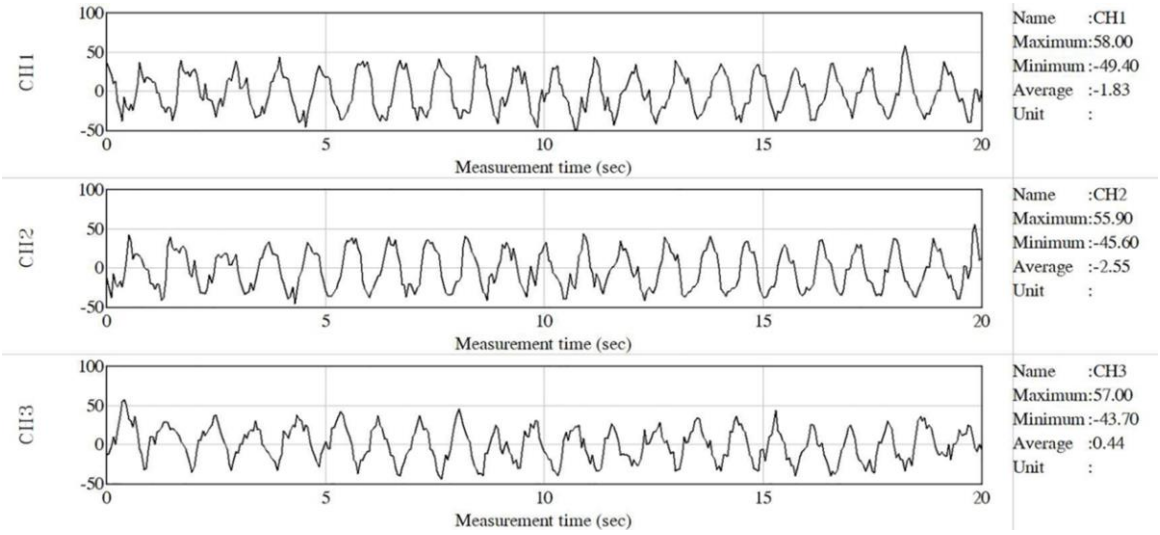

Figure 13. Variation of strain with time at the measuring points 1, 3, and 5.

Table 4. Field test results of single-sided ridger.

Detection indicator	Test value	Simulation value	Relative error (%)	Technical indicators
Torque of the compacting device torque (N m)	342	360	5	/
Firmness (kPa)	2417	2592	7	≥ 1500
Ridge height H (mm)	290	300	3	200-350
Ridge width w (mm)	360	350	3	300-400
Soil width B (mm)	480	467	3	/

test, theoretical analysis, and numerical simulation, which verified accuracy of the theoretical analysis and reliability of the numerical simulation.

CONCLUSIONS

In this paper, an integrated model was established among the key components of a single-side ridger and the soil based on EDM. To describe the mechanical behavior of soil, a comprehensive soil model was proposed by combining the plastic behavior of the soil with the cohesive force among the particles. Based on an experimental test, the reliability of the proposed model was verified.

Also, through an orthogonal test analysis, the optimal working parameters of the single-side ridger was obtained. The results showed that the relative error of soil firmness as well as working torque between the optimization analysis and EDEM virtual simulation were 1.64 and 2.89% respectively, which verified the accuracy of the optimization results.

Finally, a torque calibration test on the compacting device was designed, and a mathematical model of the torque measurement was established. Through a field test, the correctness of the virtual simulation test was determined. By comparing theoretical analyses with experimental results, the relative error of output torque of the compacting device was 4.77% and that of the firmness of the ridger was 6.77%, which met the agronomic requirements of the paddy field.

ACKNOWLEDGEMENTS

This work was supported by the National Key Research and Development Program of China [Grant Numbers: 2017YFD0701105-03].

REFERENCES

1. Asaf, Z., Rubinstein, D. and Shmulevich, I. 2006. Evaluation of Link-Track Performances Using DEM. *J. Terramechanics*, **43(2):** 141－161.
2. AshrafiZadeh, S. R. 2006. Modelling of Energy Requirements by a Narrow Tillage Tool. Doctoral Thesis, The University of Saskatchewan, Saskatoon, Canada.
3. Bery, A. A., Ismail, N. E. H. and Muztaza, N. M. 2019. Soil Properties and Behaviour Studies Using Joint-Interpretation of 4-D Electrical Resistivity Tomography and Soil Mechanics Methods in Penang, Malaysia. *EAGE-GSM 2nd Asia Pacific Meeting on Near Surface Geoscience and Engineering*, April 22-26, Kuala Lumpur, Malaysia.
4. Bravo, E. L., Tijskens E., Suarez, M. H., Gonzalez, C. O. and Ramon, H. 2014. Prediction Model for Non-Inversion Soil Tillage Implemented on Discrete. *Comput. Electron. Agric.*, **106(05):** 120-127.
5. Chen, Y., Lars, J. M. and Tavs, N. 2013. A Discrete Element Model for Soil-Sweep Interaction in Three Different Soils. *Soil Tillage Res.*, **126:** 34-41.
6. Chen, Z., Liu, C., Li, J., Zhu, J., Liu, Y., Lao, C., Feng, J., Jiang, M., Liu, C., Wang, P. and Li, Y. 2019. Mechanical Properties and Microstructures of 3D Printed Bulk

Cordierite Parts. *Ceram. Int.*, **45(15):** 19257-19267.
7. Diletta, B., Maria, B., Serena, O., Lorenzo, C., Elisa, M., Giuseppe, P., Nadia, M. and Marzia, I. 2020. Optimized Hydrolytic Methods by Response Surface Methodology to Accurately Estimate the Phenols in Cereal by HPLC-DAD: The Case of Millet. *Food Chem.*, **303:** 125393.
8. Godwin, R. J., O'Dogherty, M. J., Saunders, C. and Balafoutis, A. T. 2007. A Force Prediction Model for Mould Board Ploughs Incorporating the Effects of Soil Characteristic Properties, Plough Geometric Factors and Ploughing Speed. *Biosyst. Eng.*, **97(1):** 117－129.
9. Karmakar, S., Ashrafizadeh, S. R. and Kushwaha, R. L. 2009. Experimental Validation of Computational Fluid Dynamics Modeling for Narrow Tillage Tool Draft. *J. Terramechanics*, **46(6):** 277－283.
10. Mao, P. J., Xing, Q. Q. and Hu, C. Y. 2012. The Establishment and Analysis on Mathematical Model of Rotary Cultivator Power Consumption. *Appl. Mech. Mater.*, **159:** 366-370.
11. Shmulevich, I. 2010. State of the Art Modeling of Soil-Tillage Interaction Using Discrete Element Method. *Soil Tillage Res.*, **111(1):** 41-53.
12. Shi, L., Zhao, W. and Sun, W. 2017. Parameter Calibration of Soil Particles Contact Model of Farmland Soil in Northwest Arid Region based on Discrete Element Method. *Transactions of the Chinese Society of Agricultural Engineering*, **33(21):** 181-187. (in Chinese).
13. Ucgul, M., Fielke, J. M. and Saunders, C. 2014. 3D DEM Tillage Simulation: Validation of a Hysteretic Spring (plastic) Contact Model for A Sweep Tool Operating in A Cohesionless Soil. *Soil Tillage Res.*, **144:** 220-227.
14. Ucgul, M., Fielke, J. M. and Saunders, C. 2015. Three-Dimensional Discrete Element Modelling (DEM) of Tillage: Accounting for Soil Cohesion and Adhesion. *Biosyst. Eng.*, **129:** 298-306.
15. Wang, J., Tang, H., Wang, J., Lin, N., Huang, H. and Zhao, Y. 2017. Design and Experiment on 1DSZ-350 Type Hanging Unilateral Rotary Tillage Compacting Ridger for Paddy Field. *Transactions of the Chinese Society of Agricultural Engineering*, **33(1):** 25-37. (in Chinese).
16. Wang, J., Wang, J., Wang, F., Wang, J., Zhou, W. and Mo, Y. 2019. Optimization Design and Experiment of The Rotary Tillage Directional Soil-Collecting Device of Unilateral Ridger for Paddy Field. *International Agricultural Engineering Journal*, **28(1):** 60-70. (in Chinese).
17. Wang, J., Lin, N., Wang, J., Huang, H., Shen, H. and Yang, W. 2017. Design and Experiment on Working Dynamics Parameters of Single-side Ridger. *Transactions of the Chinese Society for Agricultural Machinery*, **48(8):** 81-86 (in Chinese).
18. Wang, J., Weng, W., Liu, J., Wang, J., Mo, Y. and Na, M. 2019. Design and Experiment of Bi-directional Ridger for Paddy Field. *Transactions of the Chinese Society for Agricultural Machinery*, **50(2):** 40-48. (in Chinese).
19. Wang, G., Guo, X., Zhao, C. and Wang, J. 2008. Soil Visual Simulation Study based on Particle System. *Transactions of the Chinese Society of Agricultural Engineering*, **24(2):** 152-158. (in Chinese).
20. Zheng, K., He, J., Li, H., Zhao, H., Hu, H. and Liu, W. 2017. Design and Experiment of Combined Tillage Implement of Reverse-rotary and Subsoiling. *Transactions of the Chinese Society for Agricultural Machinery*, **48(8):** 61-71. (in Chinese).
21. Singh, S., Tripathi, A. and Singh, A. K. 2017. Effect of Furrow Opener Design, Furrow Depth, Operating Speed on Soil Characteristics, Draft and Germination of Sugarcane. *Sugar Tech.*, **19(5):** 476-484.

بررسی عملکرد عملیاتی پشته ساز یک‌طرفه شالیزار بر مبنای روش عنصر گسسته و تایید آزمون

م. لیو، س. هو، ه. کو، و ه. کایی

چکیده

به منظور بهبود کیفیت و کارآیی یک پشته‌ساز (ridger) و بررسی اثر شرایط کار روی عملکرد آن، یک مدل کوپلینگ پیشنهاد شد که شامل اجزای کلیدی یک پشته‌ساز یک‌طرفه شالیزار و خاک و برمبنای روش عنصر گسسته بود. سپس، با پارامترهای عملیاتی پشته‌ساز به عنوان عامل‌های آزمایش وسفتی خاک و گشتاور آن به عنوان شاخص های ارزیابی، یک آزمون متعامد(orthogonal test) طراحی گردید و بهینه سازی پارامتراز طریق روش تحلیل سطح پاسخ (response surface analysis) اجرا شد. شرایط کاری بهینه به صورت زیر تنظیم شد: سرعت رو به جلو ماشین برابر ۰/۳ متر در ثانیه، سرعت چرخشی خاکورزی دورانی برابر ۵۰۰چرخش در دقیقه، و عمق کاری خاکورز دورانی برابر ۲۰۰ میلی‌متر. سفتی خاک متناظر برابر بود با ۲۵۹۲/۵۸ کیلو پاسکال و گشتاور کاری خاکورز دورانی در برش خاک و دستگاه فشرده سازی پشته به ترتیب برابر ۲۵۵/۱ نیوتن متر و۳۶۰/۱ نیوتن‌متر بود. بالاخره، یک آزمون کالیبراسیون گشتاور روی دستگاه سازنده پشته فشرده ساز اجرا گردید و مدلی از اندازه گیری گشتاور تهیه شد. با مقایسه نتایج شبیه‌سازی بهینه و نتایج آزمایش، خطای نسبی گشتاور خروجی دستگاه سازنده پشته فشرده برابر ۴/۷۷٪ و مقدار نظیر آن برای سفتی خاک پشته برابر ۶/۷۷٪ به دست آمد.